Inorganic Chemistry

Article

pubs.acs.org/IC

Selective Synthesis of Cu_2SnSe_3 and Cu_2SnSe_4 Nanocrystals

Zhen-Hua Ge,[†] James R. Salvador,[‡] and George S. Nolas*,[†]

[†]Department of Physics, University of South Florida, Tampa, Florida 33620, United States

[‡]Chemical and Materials Systems Laboratory, GM R&D Center, Warren, Michigan 48090, United States

ABSTRACT: The selective synthesis of Cu_2SnSe_3 and Cu_2SnSe_4 nanocrystals was achieved by a one-step solvothermal synthesis method. We also investigated the effects of different precursor sources and starting material concentrations on the phase purity of the products. Powder X-ray diffraction, elemental analysis, and magnetic susceptibility measurements were used to investigate the phase, purity, and homogeneity of the nanocrystals. This solvothermal approach is broadly applicable and may also be employed for the synthesis of other ternary or quaternary chalcogenide nanocrystals.

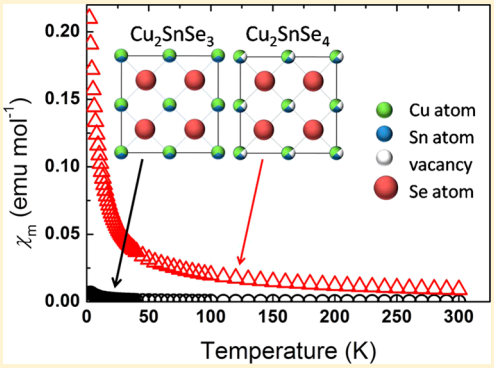

INTRODUCTION

Ternary chalcogenide semiconductors, such as Cu_2SnSe_3 and Cu_2SnSe_4, have attracted attention recently as promising thermoelectric,[1−5] solar cell,[6,7] and Li-ion battery materials.[8,9] In particular Cu_2SnSe_3, which is a p-type semiconductor with a direct band gap of 0.84 eV and a high optical absorption coefficient, has attracted considerable attention for a variety of energy conversion applications.[10−12] Cu_2SnSe_3 crystallizes in either a cubic sphalerite-like structure (space group $F\bar{4}3m$, as shown in Figure 1a)[13,14] or in a monoclinic lattice (space group Cc) with a sphalerite superstructure.[5,15,16] For cubic Cu_2SnSe_3, Cu and Sn are located on the 4*a* crystallographic site with a fractional occupancy of 0.67 and 0.33, respectively, while Se fully occupies the 4*c* site.[3,6] Cu_2SnSe_4 has a similar crystal structure (space group $F\bar{4}3m$) but contains vacancies, as shown in Figure 1b. Cu ions, vacancies, and Sn ions occupy the 4*a* site with an occupancy of 0.5, 0.25, and 0.25, respectively.[17,18] Cu_2SnSe_4 can therefore be written as $Cu_2Sn\square Se_4$, where □ denotes the cation vacancy.

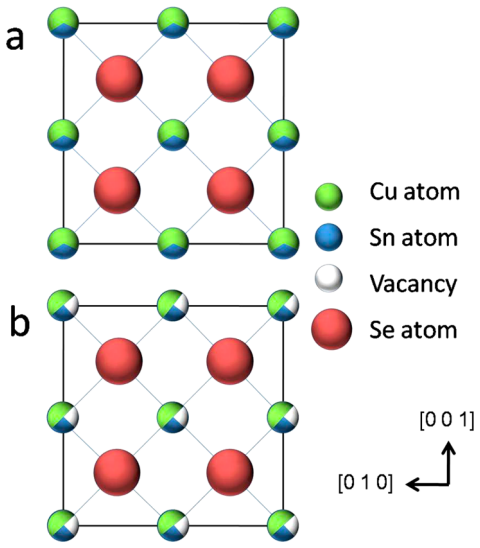

Figure 1. The crystal structure of (a) Cu_2SnSe_3 and (b) Cu_2SnSe_4.

Cu_2SnSe_3 and Cu_2SnSe_4 are typically synthesized by reacting the constituent elements at high temperatures for extended periods of time.[1,2,5] Grisaru et al.[19] synthesized Cu_2SnSe_4 nanocrystals by a microwave-assisted polyol method, while Ibanez et al.[3] recently reported the preparation of Cu_2SnSe_3 nanocrystals by a colloidal synthesis method. In this Report, Cu_2SnSe_3 and Cu_2SnSe_4 nanocrystals were selectively synthesized employing a one-step solvothermal method by varying the Cu and Sn precursors. While particle size and dispersion are not well-controlled using the reaction conditions presented here, our approach allowed for the two phases to be prepared selectively.

EXPERIMENTAL SECTION

All chemical reagents used in this study were of analytical grade and purchased form Alfa Aesar without any further purification. Cu_2SnSe_3 and Cu_2SnSe_4 nanocrystals were prepared by solvothermal synthesis. CuCl (purity 97%) and $CuCl_2$ (purity 99%) were used as Cu^+ and Cu^{2+} sources, respectively, $SnCl_2$ (purity 98%) and $SnCl_4$ (purity 98%) served as Sn^{2+} and Sn^{4+} sources, respectively, and SeO_2 (purity 99.4%) was the Se source. Information on each specimen's precursors as well as the metal source molar ratios are summarized in Table 1. Hydrazine monohydrate (purity 98%) was used as the reducing agent, and ethylene glycol (EG) was employed as the solvent. In a typical synthesis 2 mmol of CuCl, 1 mmol of $SnCl_4$, and 3 mmol of SeO_2 were added to 60 mL of EG followed by stirring for 30 min at 100 °C. Hydrazine (10 mL) was then added to the solution before stirring for

Received: January 15, 2014
Published: April 14, 2014

   dx.doi.org/10.1021/ic500100e | *Inorg. Chem.* 2014, 53, 4445−4449

Table 1. Source Species and Metal Source Ratios for All Specimens in Figure 2

specimen	source	Cu/Sn/Se ratio
a	CuCl, $SnCl_2$, SeO_2	2:1:3
b	CuCl, $SnCl_4$, SeO_2	2:1:3
c	$CuCl_2$, $SnCl_2$, SeO_2	2:1:3
d	$CuCl_2$, $SnCl_4$, SeO_2	2:1:4
e	CuCl, $SnCl_2$, SeO_2	2:1:4
f	$CuCl_2$, $SnCl_2$, SeO_2	2:1:4

another 30 min. The resulting solution was then transferred into a Teflon-lined stainless steel autoclave (100 mL capacity). The sealed autoclave was heated to 180 °C and held at this temperature for 12 h. The final solid product, which was a fine black powder, was filtered and washed with DI water and ethanol three times before drying under vacuum at room temperature. As shown in Table 1, we employed different Cu and Sn sources (Cu^+, Cu^{2+}, Sn^{2+}, and Sn^{4+}) and different Cu/Sn/Se ratios (Cu/Sn/Se = 2:1:3 and Cu/Sn/Se = 2:1:4) in this study.

The as-synthesized nanocrystals were characterized by powder X-ray diffraction (PXRD), scanning electron microscopy (SEM, JEOL JSM 6390 LV), energy dispersive X-ray spectroscopy (EDX, Inca, JEOL), transmission electron microscopy (TEM, JEOL 2100), and magnetic susceptibility measurements. Magnetic susceptibility measurements were performed on specimens with masses of ∼100 mg using a Quantum Design Magnetic Property Measurement System (MPMS). All susceptibility and magnetization measurements were performed in a gelatin capsule, which was measured prior to sample loading to establish the sample holder's background contribution. All susceptibility measurements were performed at 5 kOe between 2 and 300 K, and magnetization measurements were performed between 0 and 50 kOe from 5 to 25 K in 5 K increments and then from 25 to 300 K in 25 K increments. The core electron diamagnetic contribution was applied to data that was already corrected for the sample container contribution, with values taken from reference 20.

RESULTS

Figure 2 shows the PXRD patterns of specimens **a** through **f** obtained when different Cu and Sn sources as well as different raw material ratios were used. The PXRD patterns for all the specimens are similar, and there are no impurities observed in the PXRD patterns for specimens **a**, **b**, **c**, and **f**. For specimens **e** and **d**, elemental Se was identified as an impurity. The reflection intensity ratio I(111)/I(220) found in specimen **f** is different from that of the other specimens' PXRD powder patterns. This difference in intensity ratio for specimen **f** is suggestive of the formation of Cu_2SnSe_4. However, the unambiguous differentiation of the Cu_2SnSe_3 and Cu_2SnSe_4 phases by PXRD alone is difficult because of the similarity of their respective patterns.[21−24]

To more conclusively differentiate Cu_2SnSe_3 and Cu_2SnSe_4 other measurements were performed. Figure 3 shows SEM images and EDX results of specimens **a** and **f**. From the SEM analyses both specimens **a** and **f** have very small particle sizes. The EDX results indicate a Cu/Sn/Se ratio close to 2:1:3 for specimen **a** and a ratio close to 2:1:4 for specimen **f**. To obtain more information about the particle size, TEM images were obtained. Figure 4a,b shows the morphology of specimen **a**, and Figure 4d,e shows the morphology of specimen **f**. The average crystal size for specimen **a** (Cu_2SnSe_3) was approximately 25 nm with a relatively narrow size dispersion, as shown in Figure 4c. The average crystal size for specimen **f** (Cu_2SnSe_4) was approximately 45 nm with a larger particle size dispersion as compared to specimen **a**, as shown in Figure 4f. A possible

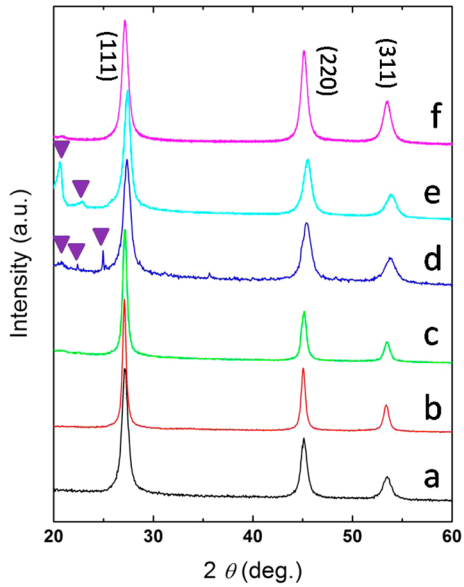

Figure 2. PXRD patterns of the specimens obtained with different precursor material ratios and species. (a) Cu/Sn/Se = 2:1:3, Cu^+ and Sn^{2+}; (b) Cu/Sn/Se = 2:1:3, Cu^+ and Sn^{4+}; (c) Cu/Sn/Se = 2:1:3, Cu^{2+} and Sn^{2+}; (d) Cu/Sn/Se = 2:1:4, Cu^+ and Sn^{2+}; (e) Cu/Sn/Se = 2:1:4, Cu^{2+} and Sn^{2+}; (f) Cu/Sn/Se = 2:1:4, Cu^{2+} and Sn^{4+}. The ▼ denotes the Se impurity peaks.

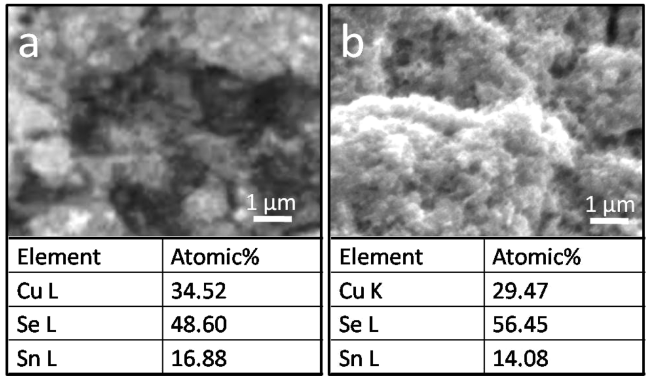

Element	Atomic%
Cu L	34.52
Se L	48.60
Sn L	16.88

Element	Atomic%
Cu K	29.47
Se L	56.45
Sn L	14.08

Figure 3. SEM images and EDX results of (a) Cu_2SnSe_3 and (b) Cu_2SnSe_4.

explanation for the larger average crystal size and higher dispersion of specimen **f** may be that the vacancies improve the growth rate of the crystals during the solvothermal process, leading to higher rates of crystal growth and Otswald ripening.[25,26] As a result, for the same reaction temperature and holding time Cu_2SnSe_4 nanocrystals are larger in size. Any size difference due to the different precursors may be due to a difference in growth dynamics for these two compositions; however, further work is needed to completely investigate these growth dynamics. The main objective of this work, however, is not morphological control of the final products but rather the demonstration of selective phase formation though the judicious selection of reactants and precursors by solvothermal synthesis.

Magnetic susceptibility measurements were also performed on specimens **a** and **f**, which will henceforth be referred to by their EDX-derived compositions as Cu_2SnSe_3 and Cu_2SnSe_4, respectively. The molar susceptibility (χ_m) as a function of temperature is shown in Figure 5 and indicates that the

dx.doi.org/10.1021/ic500100e | Inorg. Chem. 2014, 53, 4445−4449

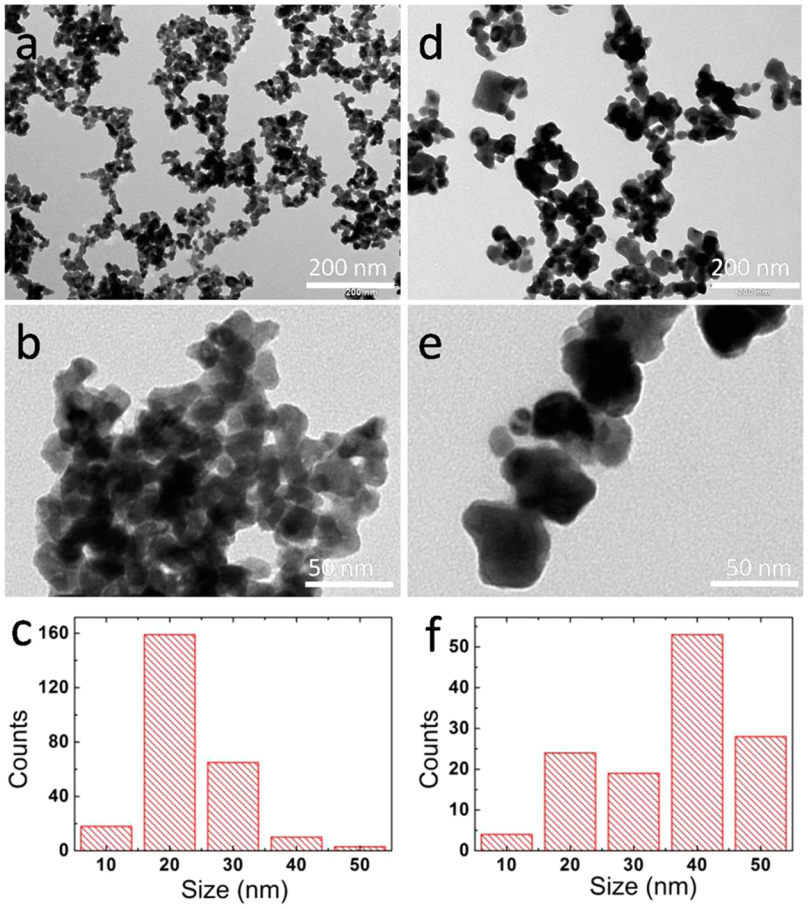

Figure 4. TEM images of (a, b) Cu_2SnSe_3 and (c) the corresponding estimated particle size distribution. TEM images of (d, e) Cu_2SnSe_4 and (f) the corresponding estimated particle size distribution.

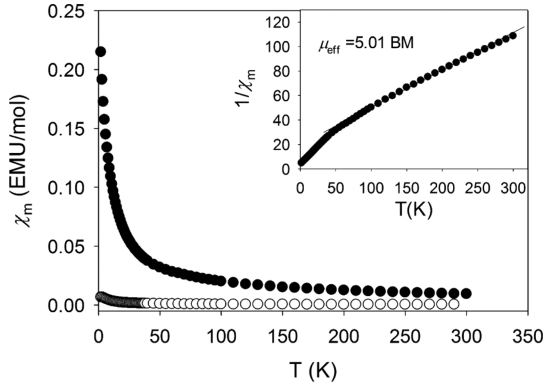

Figure 5. Temperature-dependent magnetic susceptibility of Cu_2SnSe_4 (●) and Cu_2SnSe_3 (○). (inset) The inverse susceptibility as a function of temperature for Cu_2SnSe_4.

Cu_2SnSe_4 nanocrystals are paramagnetic due to Cu^{2+}, in agreement with previous studies.[18] A plot of the $1/\chi_m$ values as a function of temperature leads to a nearly linear dependence, in accordance with the Curie−Weiss relationship, as seen in the inset of Figure 5. Careful inspection of the inset plot finds a change in slope of the $1/\chi_m$ versus T data below 50 K. This is likely due to the fact that below this temperature there is a nonlinear dependence of the moment as a function of applied magnetic field, whereas above this temperature a linear dependence is observed. The slope of the $1/\chi_m$ versus T relation between 50 and 300 K yields an effective magnetic moment (μ_{eff}) of 5.01 μ_B per formula unit (Cu_2SnSe_4). Since we expect two Cu^{2+} ions per formula the total μ_{eff} can be decomposed to approximately 3.55 μ_B per Cu^{2+} ion. This is significantly higher than the 1.73 μ_B per ion that would be expected from a spin-only magnetic moment, and in fact a μ_{eff} = 3.55 μ_B is the value expected for a Cu^{2+} ion with full orbital angular moment contribution to the magnetic moment.[27] It is known that transition-metal ions in tetrahedral coordination environments experience weaker quenching of orbital angular momentum as compared to those in octahedral coordination, and this fact may account for part of the larger-than-expected μ_{eff} value observed in Cu_2SnSe_4.[28] In addition we cannot rule out the possibility of small amounts of $CuCl_2$ or CuO in the specimen also contributing to the unusually large μ_{eff}. For Cu_2SnSe_3 copper is expected to be monovalent, and thus Cu_2SnSe_3 nanocrystals should be diamagnetic.[29] In Figure 5, however, Cu_2SnSe_3 shows weak paramagnetic behavior, indicating the presence of a trace amount of Cu_2SnSe_4 or other paramagnetic impurity phase. Plotting $1/\chi_m$ versus T for the Cu_2SnSe_3 composition does not yield a straight a line, indicating that, while the specimen is paramagnetic, it does not conform to the Currie-Weiss relationship. We can conclude that the paramagnetic response is likely due to impurity phases, but the role and effects of vacancies and other defects in Cu_2SnSe_3 on the resulting magnetic properties are unknown, and their contribution to the paramagnetic nature of this sample cannot be ruled out. However, given the diminutive nature of the susceptibility of the Cu_2SnSe_3 phase as compared

dx.doi.org/10.1021/ic500100e | Inorg. Chem. 2014, 53, 4445−4449

to Cu_2SnSe_4 we can conclude that the latter phase exhibits paramagnetic behavior consistent with it containing a vast majority of paramagnetic Cu^{2+} ions while the former phase contains predominately diamagnetic Cu^+.

DISCUSSION

On the basis of the above results Cu_2SnSe_3 and Cu_2SnSe_4 nanocrystals synthesized by the same solvothermal method with the same reaction parameters were obtained by varying the Cu and Sn sources. When Cu^+/Sn^{2+}, Cu^{2+}/Sn^{2+}, or Cu^+/Sn^{4+} were used as the Cu and Sn sources with a Cu/Sn/Se ratio of 2:1:3, Cu_2SnSe_3 nanocrystals were obtained. When Cu^+/Sn^{2+} or Cu^{2+}/Sn^{2+} were used as the Cu and Sn sources with a Cu/Sn/Se ratio of 2:1:4, Cu_2SnSe_3 nanocrystals were again formed, together with elemental Se as an impurity. Only when Cu^{2+} and Sn^{4+} were used in a molar ratio of 2:1:4 were Cu_2SnSe_4 nanocrystals obtained. This indicates that the Cu and Sn sources can be used to selectively synthesize the desired product. According to standard electrode potentials $E^{\circ}_{Cu^{2+}/Cu^+}$ = 0.17 eV and $E^{\circ}_{Sn^{4+}/Sn^{2+}}$ = 0.15 eV, Sn^{2+} can reduce Cu^{2+} to Cu^+ during the solution mixing process.[30] Combining the above results it is clear that when there is Cu^+ in solution before adding hydrazine, Cu_2SnSe_3 is formed preferentially, and when there is Cu^{2+} in solution before adding hydrazine Cu_2SnSe_4 is favored. This is in agreement with the expected valence state of copper in Cu_2SnSe_3 (Cu^+) and Cu_2SnSe_4 (Cu^{2+}). In keeping with the standard electrode potentials,[31] Cu^+ and Cu^{2+} in a water solution can be reduced to copper(0) by most commonly used reducing agents; however, in many cases Cu_2O is formed when the solution is alkaline.[32,33] In our case SeO_2 will be reduced to Se by hydrazine;[34] therefore, Cu_2Se was formed (instead of Cu_2O) due to the presence of Se. Both Cu^+ and Cu^{2+} form Cu_2Se in solution, although Cu^+ will consume less hydrazine compared to Cu^{2+} due to its lower valence.[35]

These results demonstrate the selective nature of the solvothermal synthesis method in preferentially synthesizing Cu_2SnSe_3 or Cu_2SnSe_4 on the basis of the oxidation state of the precursor salts and their molar ratios. This approach can be used to synthesize other ternary or quaternary chalcogenides, for example, Cu_2SnS_3 or $Cu_2MnSnSe_4$.

CONCLUSION

Cu_2SnSe_3 and Cu_2SnSe_4 nanocrystals were successfully synthesized by a solvothermal method. When Cu^+ is the Cu source in solution before adding the reducing agent, with a Cu/Sn/Se ratio of 2:1:3, Cu_2SnSe_3 nanocrystals were obtained. When Cu^{2+} is the Cu source in solution prior to adding hydrazine, with a Cu/Sn/Se ratio of 2:1:4, Cu_2SnSe_4 nanocrystals were obtained. It was also observed that Sn^{2+} can reduce Cu^{2+} to Cu^+ during the solution mixing process to yield Cu_2SnSe_3. The average crystallite size of Cu_2SnSe_3 was 25 nm, while that of Cu_2SnSe_4 was 45 nm. Magnetic susceptibility measurements showed Cu_2SnSe_4 to be strongly paramagnetic, in contrast to Cu_2SnSe_3, a result that is in agreement with previous results.[18] We demonstrated that a simple solvothermal route can be employed in selectively synthesizing Cu_2SnSe_3 and Cu_2SnSe_4 nanocrystals by controlling the Cu source species and the Cu/Sn/Se ratio.

AUTHOR INFORMATION

Corresponding Author

*E-mail: gnolas@usf.edu.

Notes

The authors declare no competing financial interest.

ACKNOWLEDGMENTS

This work was supported by the National Science Foundation and Department of Energy Partnership on Thermoelectric Devices for Vehicle Applications (Grant No. 1048796). J.R.S. would like to thank J. F. Herbst and M. W. Verbrugge for their continued support. Financial support for work at GM comes from the Department of Energy under corporate agreement DE-FC26-04NT 42278.

REFERENCES

(1) Shi, X. Y.; Xi, L. L.; Fan, J.; Zhang, W. Q.; Chen, L. D. *Chem. Mater.* **2010**, *22*, 6029−6031.
(2) Fan, J.; Liu, H. L.; Shi, X. Y.; Bai, S. Q.; Shi, X.; Chen, L. D. *Acta Mater.* **2013**, *61*, 4297−4304.
(3) Ibanez, M.; Cadavid, D.; Anselmi-Tamburini, U.; Zamani, R.; Gorsse, S.; Li, W. H.; Lopez, A. M.; Morante, J. R.; Arbiol, J.; Cabot, A. *J. Mater. Chem. A* **2013**, *1*, 1421−1426.
(4) Skoug, E. J.; Cain, J. D.; Morelli, D. T. *J. Electron. Mater.* **2012**, *41*, 1232−1236.
(5) Fan, J.; Carrillo-Cabrera, W.; Akselrud, L.; Antonyshyn, I.; Chen, L. D.; Grin, Y. *Inorg. Chem.* **2013**, *52*, 11067−11074.
(6) Ahmadi, M.; Pramana, S. S.; Batabyal, S. K.; Boothroyd, C.; Mhaisalkar, S. G.; Lam, Y. M. *Inorg. Chem.* **2013**, *52*, 1722−1728.
(7) Kim, K. M.; Tampo, H.; Shibata, H.; Niki, S. *Thin Solid Films* **2013**, *536*, 111−114.
(8) Qu, B.; Li, H.; Zhang, M.; Mei, L.; Chen, L.; Wang, Y.; Li, Q.; Wang, T. *Nanoscale* **2011**, *3*, 4389−4393.
(9) Qu, B.; Zhang, M.; Lei, D.; Zeng, Y.; Chen, Y.; Chen, L.; Li, Q.; Wang, Y.; Wang, T. *Nanoscale* **2011**, *3*, 3646−3651.
(10) Zhai, Y.-T.; Chen, S.; Yang, J.-H.; Xiang, H.-J.; Gong, X.-G.; Walsh, A.; Kang, J.; Wei, S.-H. *Phys. Rev. B: Condens. Matter Mater. Phys.* **2011**, *84*, 075213.
(11) Chandra, G. H.; Kumar, O. L.; Rao, R. P.; Uthanna, S. *J. Mater. Sci.* **2011**, *46*, 6952−6959.
(12) Marcano, G.; Rincón, C.; De Chalbaud, L. M.; Bracho, D. B.; Pérez, G. S. *J. Appl. Phys.* **2001**, *90*, 1847−1853.
(13) Palatnik, L. S.; Komnik, Y. F.; Belova, E. K.; Adroschenko, L. V. *Kristallografiya* **1961**, *6*, 960−964.
(14) Sharma, B. B.; Ayyar, R.; Singh, H. *Phys. Status Solidi A* **1977**, *40*, 691−696.
(15) Delgado, G. E.; Mora, A. J.; Marcano, G.; Rincón, C. *Mater. Res. Bull.* **2003**, *38*, 1949−1955.
(16) Gulay, L. D.; Daszkiewicz, M.; Ostapyuk, T. A.; Klymovych, O. S.; Zmiy, O. F. *Acta Crystallogr., Sect. C: Cryst. Struct. Commun.* **2010**, *66*, 158−160.
(17) Delgado, J. M. *Inst. Phys. Conf. Ser.* **1998**, *152*, 45.
(18) Marcano, G.; Rincón, C.; Marín, G.; Tovar, R.; Delgado, G. *J. Appl. Phys.* **2002**, *92*, 1811.
(19) Grisaru, H.; Pol, V. G.; Gedanken, A.; Nowik, I. *Eur. J. Inorg. Chem.* **2004**, *9*, 1859−1864.
(20) Bain, G. A.; Berry, J. H. *J. Chem. Educ.* **2008**, *85*, 532−536.
(21) Li, B.; Xie, Y.; Huang, J.; Qian, Y. *Solid State Ionics* **1999**, *126*, 359−363.
(22) Li, Q.; Ding, Y.; Liu, X.; Qian, Y. *Mater. Res. Bull.* **2001**, *36*, 2649−2656.
(23) Li, B.; Xie, Y.; Huang, J.; Qian, Y. *Solid State Ionics* **1999**, *126*, 359−362.
(24) Liu, X.-Z.; Chen, L.; Fang, D.-W.; Zhao, C.-M.; Li, J.; Zang, S.-L. *Chin. J. Inorg. Chem.* **2005**, *21*, 1451−1456.
(25) Hafeez, M.; Zhai, T.; Bhatti, A. S.; Bando, Y.; Golberg, D. *Cryst. Growth Des.* **2012**, *12*, 4935−4943.
(26) Hubbard, A. T. *Encyclopedia of Surface and Colloid Science;* CRC Press: Boca Raton, FL, 2004; p 4230.
(27) Kittel, C. *Introduction to Solid State Physics,* 7th ed.; Wiley: Hoboken, NJ, 1996; p 426.

(28) Figgis, B. N.; Lewis, J. The Magnetochemistry of Complex Compounds. In *Modern Coordination Chemistry;* Lewis, J., Wilkins, R. G., Eds.; Wiley: Hoboken, NJ, 1960; p 415.
(29) Romero, H.; Nieves, L.; Chourio, M.; Echeverria, R.; Carreron, I.; Ramirez, B.; Zysler, R. *J. Magn. Magn. Mater.* **2004**, *272−276*, E1567−E1569.
(30) Hu, H.-M.; Deng, C.-H.; Mei, S.; Zhang, K.-H. *Chin. J. Inorg. Chem.* **2010**, *26*, 1189−1194.
(31) Lur'e, Y. Y. Spravochnik Po Analiticheskoi Khimii. In *Analytical Chemistry Handbook;* Khimiya: Moscow, 1978; p 48.
(32) Dong, Y.; Li, Y.; Wang, C.; Cui, A.; Deng, Z. *J. Colloid Interface Sci.* **2001**, *243*, 85−89.
(33) Du, F.; Liu, J.; Guo, Z. *Mater. Res. Bull.* **2009**, *44*, 25−29.
(34) Ge, Z.; Wei, K.; Nolas, G. S. *Phys. Status Solidi A* **2013**, *210*, 2725−2728.
(35) Wang, J.-S.; Matyjaszewski, K. *Macromolecules* **1995**, *28*, 7901−7910.

dx.doi.org/10.1021/ic500100e | *Inorg. Chem.* 2014, 53, 4445−4449